

Article

Quantifying Climatic Impact on Reference Evapotranspiration Trends in the Huai River Basin of Eastern China

Meng Li ^{1,†} , Ronghao Chu ^{1,*,†} , Shuanghe Shen ^{1,*} and Abu Reza Md. Towfiqul Islam ² 

¹ Key Laboratory of Meteorological Disaster, Ministry of Education (KLME), Joint International Research Laboratory of Climate and Environment Change (ILCEC), Collaborative Innovation Center on Forecast and Evaluation of Meteorological Disasters (CIC-FEMD), Jiangsu Key Laboratory of Agricultural Meteorology, College of Applied Meteorology, Nanjing University of Information Science & Technology, Nanjing 210044, China; lm_nuist@163.com

² Department of Disaster Management, Begum Rokeya University, Rangpur 5400, Bangladesh; towfiq_dm@brur.ac.bd

* Correspondence: ronghao_chu@163.com (R.C.); yqzhr@nuist.edu.cn (S.S.); Tel.: +86-187-5209-3867 (R.C.); +86-136-0146-6916 (S.S.)

† These authors contributed equally to this work.

Received: 18 December 2017; Accepted: 30 January 2018; Published: 2 February 2018

Abstract: Reference evapotranspiration (ET_{ref}) is an important study object for hydrological cycle processes in the context of drought-flood risks of the Huai River Basin (HRB). In this study, the FAO-56 Penman–Monteith (PM) model was employed to calculate seasonal and annual ET_{ref} based on 137 meteorological station data points in HRB from 1961 to 2014. The Mann–Kendall (MK) trend analysis was adopted together with Theil–Sen’s estimator to detect tendencies of ET_{ref} and climate factors. Furthermore, a developed differential equation method based on the FAO-56 PM model was applied to quantify the sensitivities of ET_{ref} to meteorological factors and their contributions to ET_{ref} trends. The results showed that the ET_{ref} demonstrated a strong spatially heterogeneity in the whole HRB at each time scale. ET_{ref} showed a significant decreasing trend in the upper-middle HRB and Yi-Shu-Si River Basin, especially at the annual time scale, in growing season and summer, while a generally increasing trend in ET_{ref} was detected in the lower HRB, and the significance only showed in spring. These phenomena could be reasonably explained by a significantly increasing mean temperature (TA), a significantly decreasing wind speed (WS), solar radiation (SR), and a slightly decreasing relative humidity (RH). The most sensitive factor to ET_{ref} was RH in most sub-regions and most time scales, except in the growing season and summer. Based on the developed differential equation method, the dominant factor of the decreasing ET_{ref} was WS in the annual time scale, spring, autumn, and winter in most sub-regions, except the lower HRB, which then shifted to SR in the growing season and summer. However, in the lower HRB, the significantly decreasing RH was the most dominant factor, especially in the annual time scale, growing season, and spring, which might be responsible for the slightly increasing ET_{ref} there.

Keywords: reference evapotranspiration; sensitivity coefficient; contribution; Huai River Basin; differential equation method

1. Introduction

Evapotranspiration (ET), as a vital component in water cycle, is a critical variable for hydrometeorological studies [1]. At the same time, the reference evapotranspiration (ET_{ref}) refers to the evapotranspiration (ET) from the crop reference surface, which has a $70 \text{ s}\cdot\text{m}^{-1}$ unified surface resistance, a 0.12 m hypothetical reference height, and a 0.23 albedo [2,3]. It determines the surface runoff,

soil moisture, groundwater recharge, as well as the crop growth [4], and plays a crucial role in climatology, hydrological processes, irrigation management, planning, and scheduling [5,6]. Moreover, the global average temperature across the land and ocean surface increased by 0.85 °C from 1880 to 2012 [7]. In the context of global warming, the hydrological cycle processes were altered dramatically in many parts of the world. Furthermore, crop productivity was also influenced by the climate change to some extent [8].

Nowadays, several methods have been developed to compute the ET_{ref} presently, mainly based on the water budget, mass-transfer, radiation, and temperature [9]. Among these methods, the FAO-56 PM model, as proposed by the Food and Agriculture Organization (FAO), is universally accepted as the most precise one to estimate the reference evapotranspiration [2]. However, as global warming has become a historical truth and scientific fact in recent decades, the ET_{ref} , as well as pan evaporation (E_{pan}), exhibited a significant downward trend globally [10–12]. Meanwhile, the decreasing trend of ET_{ref} or E_{pan} generally appears to be an “evaporation paradox” [13], one of the most controversial scientific problems. Likewise, decrease of ET_{ref} trends has been discovered from many areas in China [14–16]. Apart from these reports, many researchers have shown the increase of ET_{ref} in various places around the world, including Asia [17,18] and Europe [19,20]. These results are echoed with similar observations in China; for instance, the upper, middle, and entire Yellow River Basin [21], Jianghuai area, and Sunan area in Jiangsu province [16], and most parts of Wei River Basin [22]. Additionally, during the past several decades, a significant number of investigators have identified the influence of meteorological parameters to the changing ET_{ref} [23–25]. ET_{ref} variation, and its spatiotemporal distribution, are not only influenced by the increasing air temperature, but also by some primary climate factors, namely, relative humidity, wind speed, and solar radiation. Therefore, it is an important study object to quantify the influences of various climate factors on the ET_{ref} change, especially in the background of global climatic change [26].

Different attribution analysis methods are widely employed for calculating contributions of climate factors to ET_{ref} variations. The sensitivity coefficients method, multiple regressions, and the detrending method are the three most used attribution analysis methods. Mccuen [27] first introduced the sensitivity coefficient method to recognize the relative change of ET_{ref} according to meteorological factors. Later, Yin et al. [28] and Huo et al. [14] successfully applied this approach to identify the anticipated change of ET_{ref} caused by variations of climate factors. Similarly, other scholars in China revealed relative contributions of climate variables to the ET_{ref} by employing sensitivity coefficient analysis [29–31]. Contrarily, Ye et al. [32], Shan et al. [33], and Wang et al. [34] adopted the multiple regression analysis method to establish the relations between the ET_{ref} (dependent variable) and climate parameters (independent variables), then determined relative contributions of climatic variables to the ET_{ref} trends. Recently, the stepwise regression analysis and partial correlation analysis were employed for investigating influences of climate factors to ET_{ref} change in the West Liao River Basin [35]. Moreover, the detrending method, a statistical and mathematical modeling approach, first proposed by Xu et al. [1], was used to evaluate changes of ET_{ref} to the related climate factors. This method has been applied to assess the influences of climate factors to the ET_{ref} change in various regions of China such as the Heihe River Basin [36], Yellow River Basin [37], northwest area of China [14], Jiangsu province of Eastern China [16], and also other countries like Iran [38]. The above-mentioned attribution analysis methods only consider the relative contributions of meteorological factors to ET_{ref} changes, however, actual contributions to the ET_{ref} changes are still unclear and needed to be explored. Roderick et al. [39] have pioneered the use of a physical and mathematical model—namely, the PenPan model—which is based on mass and energy balances, to evaluate the contributions of climatic parameters to E_{pan} . In the PenPan model, the E_{pan} trend is divided into the radiative and aerodynamic items. Furthermore, the E_{pan} trend caused by the aerodynamic item is also partitioned into three components: wind speed, vapor pressure deficit, and mean air temperature. Various researchers have adopted this differential equation method to quantitatively analysis the change in E_{pan} [40–42], however, few studies have used it for ET_{ref} analysis. Additionally, the PenPan model was employed by Liu and Zhang [43] to determine the changes in ET_{ref} in Northwest China. Some previous studies [40,43] also adopted the differential equation method based on the FAO-56 PM model to

determine contributions of four meteorological variables (mean temperature, actual vapor pressure, solar radiation, and wind speed) to the ET_{ref} trend. However, the actual vapor pressure is not an independent variable, but a dependent variable on mean air temperature and relative humidity. Thus, considering the independence of each selected variable, we decided to replace the actual vapor pressure with the relative humidity in this study, and hypothesize that the combination of the four new variables is reasonable, then we verify this hypothesis. Considering the accuracy and reliability of the differential equation method, we developed this method based on the FAO-56 PM model to verify our hypothesis, and also to quantify the attribution of each climatic factor to ET_{ref} trends in the Huai River Basin (HRB).

HRB, adjoining the Yangtze River Delta, as a fast economic growth region in Eastern China, is susceptible to confronting extreme weather and hydro-meteorological events, particularly flood calamities [44]. These climatic challenges will exacerbate a potential impact on the hydrometeorology of the HRB. Moreover, the HRB is in a decisive status in the agricultural production of China and the density of population here is nearly five-fold higher than the national average level. However, there are only a few studies about long-term quantitative attribution analysis of meteorological factors to the ET_{ref} in the HRB of Eastern China. Thus, research on the climate factors attribution analysis to regional ET_{ref} changes is needed to understand the spatiotemporal trends of regional climatic change and the influence of climatic change on agricultural irrigation scheduling.

Based on the hypotheses above, the aims of this study are (1) to estimate the ET_{ref} changes in seasonal and annual time scales in HRB from 1961 to 2014 by means of the FAO-56 PM model; (2) to identify the spatiotemporal tendencies of seasonal and annual ET_{ref} series together with its relative climate factors through the Mann–Kendall (MK) test, together with Sen's slope estimator, over the past 54 years; (3) to explore the sensitivities of ET_{ref} to each climatic factor at seasonal and annual time scales using sensitivity coefficients analysis; and (4) to quantify the contributions from climate factors to ET_{ref} change trends by using a developed differential equation model and its spatial distribution patterns in seasonal and annual time scales. This study would offer a theoretical guidance for the management of agricultural irrigation resource usage, crop production, as well as the countermeasure to climatic change perspective in this vital region.

2. Materials and Methods

2.1. Study Area

The HRB is located between the Yangtze River and Yellow River Basin in Eastern China ($111^{\circ}55' E$ – $121^{\circ}25' E$ and $30^{\circ}55' N$ – $36^{\circ}36' N$) and has a watershed area of 270,000 km². The length of the main stream is about 1000 km and the total river fall is about 200 m (Figure 1). Meanwhile, the HRB is situated in the climatic transition zone, which is recognized as the demarcation line (zero isotherm) between warm temperate and northern subtropical zones in China, accompanied with four distinctive seasons and moderate climate. The annual average precipitation is about 911 mm, with an uneven distribution pattern. More than 50% of the rainfall is concentrated during the monsoon season from June to September, accompanied by complex weather systems. Furthermore, the HRB is the most densely populated area and also a major grain-producing base in Eastern China [45], with the main crops—including wheat, rice, maize, potato, soybean, cotton, and canola—accounting for 17.3% of the total national grain yield.

2.2. Data Source

The datasets employed in the present study are mainly daily weather data obtained from 137 stations during 1961–2014 in the HRB, including the daily mean temperature (TA , °C), maximum temperature (T_{max} , °C) and minimum temperature (T_{min} , °C), relative humidity (RH , %), wind speed at 10 m (u_{10} , m·s⁻¹), and sunshine duration (SD , h). We obtained the weather data from the National Meteorological Information Center (NMIC) of the China Meteorological Administration (CMA)

(<http://data.cma.cn/site/index.html>). The censored data are complemented through establishing linear interpolation between the neighboring weather stations. In this study, we defined five seasons as the growing season (April–October), spring (March–May), summer (June–August), autumn (September–November), and winter (December–February of the following year). The DEM (digital elevation model) datasets of 90 m spatial resolution (Figure 1) were acquired from the Internet (<http://srtm.csi.cgiar.org/>).

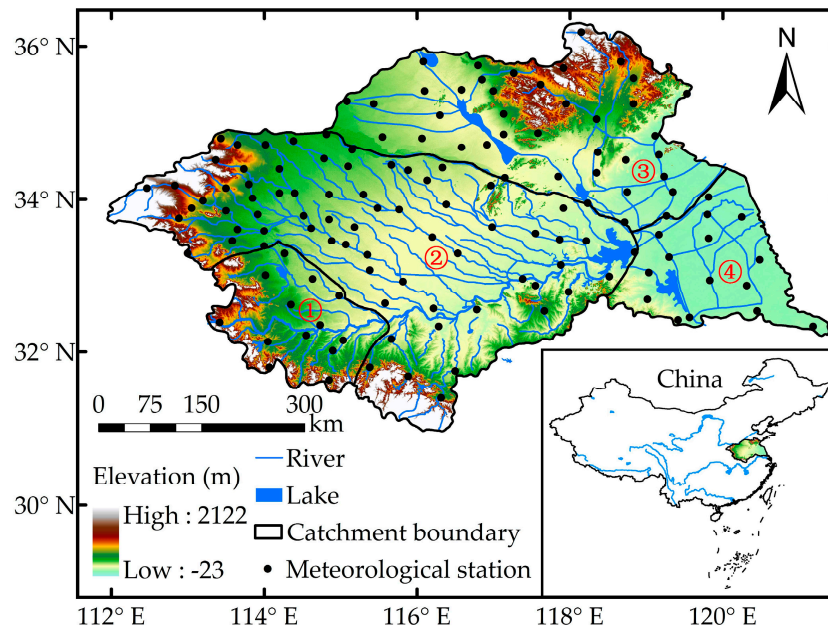


Figure 1. The location of the Huai River Basin (HRB) in China and its spatial distributions of the elevation, meteorological stations and the river system, four sub-regions represent ①: Upper HRB, ②: Middle HRB; ③: Yi-Shu-Si River Basin; and ④: Lower HRB, respectively.

2.3. Reference Evapotranspiration Calculation

The FAO-56 Penman–Monteith (PM) model proposed by the Food and Agriculture Organization (FAO) has been regarded as an international recognized method to calculate ET_{ref} [2]. The FAO-56 PM model has a full theoretical basis which shows high accuracy [16]. The detailed formula is given as

$$ET_{ref} = \frac{0.408\Delta(R_n - G) + \gamma \frac{900}{T+273} u_2 (e_s - e_a)}{\Delta + \gamma(1 + 0.34u_2)} \quad (1)$$

where ET_{ref} refers to the daily reference crop evapotranspiration ($\text{mm}\cdot\text{day}^{-1}$), Δ refers to the slope of vapor pressure curve ($\text{kPa}\cdot\text{C}^{-1}$), R_n refers to the net radiation at the crop height ($\text{MJ}\cdot\text{m}^{-2}\cdot\text{day}^{-1}$), G refers to the soil heat flux density ($\text{MJ}\cdot\text{m}^{-2}\cdot\text{day}^{-1}$), γ refers to the psychrometric constant ($\text{kPa}\cdot\text{C}^{-1}$), T refers to the daily mean air temperature at 2 m ($^{\circ}\text{C}$), u_2 refers to the wind speed at two-meter height ($\text{m}\cdot\text{s}^{-1}$), e_s and e_a refer to the saturation vapor pressure (kPa) and the actual vapor pressure (kPa), respectively.

For the convenience of ET_{ref} calculation, a conversion formula for wind speed was proposed by Allen et al. [2] as

$$u_2 = u_z \frac{4.87}{\ln(67.8z - 5.42)} \quad (2)$$

where u_2 refers to wind speed at two-meter height ($\text{m}\cdot\text{s}^{-1}$), u_z refers to the wind speed at z meters above ground level.

Due to the lack of measured solar radiation (R_s) data ($\text{MJ}\cdot\text{m}^{-2}\cdot\text{day}^{-1}$), R_s is often calculated through sunshine hours, combed with the Angstrom formula [46]

$$R_s = \left(a_s + b_s \frac{n}{N} \right) R_a \quad (3)$$

where R_s refers to daily total solar radiation ($\text{MJ}\cdot\text{m}^{-2}\cdot\text{day}^{-1}$), R_a refers to extraterrestrial radiation ($\text{MJ}\cdot\text{m}^{-2}\cdot\text{day}^{-1}$), n refers to daily sunshine hours (h), N refers to maximum possible sunshine hours (h), a_s and b_s are regression coefficients, according to Chen et al. [47], the values were set to 0.19 and 0.53, respectively [16].

Meanwhile, some sunshine duration data were missing in several inland stations of the HRB. In this regard, the radiation equation proposed by Hargreaves and Samani [48] was employed for calculating solar radiation (R_s) through T_{max} and T_{min} as

$$R_s = k_{RS} \times \sqrt{(T_{max} - T_{min})} \times R_a \quad (4)$$

where k_{RS} refers to the empirical coefficient and usually adopted the value of 0.16 for inland regions [48–50]. In order to verify the availability of the Hargreaves–Samani method, complete sunshine duration (SD) datasets of 39 meteorological stations located in the upper and middle HRB were employed in this study. The estimated SR and ET_{ref} calculated with Hargreaves–Samani (HS) method were compared with that calculated with SD during 1961–2014. The specific accuracy test can be found in Appendix A.

Finally, the net radiation (R_n) is estimated by

$$R_n = R_{ns} - R_{nl} \quad (5)$$

$$R_{ns} = (1 - \alpha) R_s \quad (6)$$

$$R_{nl} = \sigma \left(\frac{T_{max,K}^4 + T_{min,K}^4}{2} \right) (0.34 - 0.14 \sqrt{e_a}) \left(1.35 \frac{R_s}{R_{s0}} - 0.35 \right) \quad (7)$$

in which R_{ns} refers to the incoming net shortwave radiation ($\text{MJ}\cdot\text{m}^{-2}\cdot\text{day}^{-1}$), α refers to the albedo of reference crop (value of 0.23), R_{nl} refers to the net outgoing long-wave radiation ($\text{MJ}\cdot\text{m}^{-2}\cdot\text{day}^{-1}$), σ refers to the Stefan–Boltzmann constant ($4.903 \times 10^{-9} \text{ MJ}\cdot\text{K}^{-4}\cdot\text{m}^{-2}\cdot\text{day}^{-1}$), $T_{max,K}$ represents the maximum absolute temperature during 24 h ($\text{K} = ^\circ\text{C} + 273.16$), $T_{min,K}$ represents the minimum absolute temperature during 24 h ($\text{K} = ^\circ\text{C} + 273.16$), and R_{s0} refers to clear-sky radiation. Furthermore, more specific approach procedures are provided in Allen et al.'s literature [2].

2.4. Trend Analysis

The worldwide recommended nonparametric test, Mann–Kendall (MK) test, was built to calculate the significance of a trend in hydro-meteorological time series [51,52]. The MK test is employed in this research to analyze temporal change trends of ET_{ref} and related meteorological variables [53–55]. It has an advantage which lies in its ability to test the linearity of a trend [31].

In order to identify slopes of ET_{ref} trends and climate factors, Theil–Sen's estimator [55,56], a widely applied method to calculate the slope magnitude of the trend line, was adopted in this study

$$\beta = \text{Median} \left(\frac{x_j - x_i}{j - i} \right), \forall 1 < i < j \quad (8)$$

where β refers to the estimated trend slope of the data series, x_j and x_i refer to the sequential data corresponding to time j and i , respectively.

Prior to applying the M–K test in this study, a pre-whitening method should be employed to eliminate the effect of a serial correlation on the trend value [57]. Yue et al. [58] improved this method

and proposed an alternative approach, namely TFPW (trend-free pre-whitening), which is widely applied in many related study areas [17,30,59].

2.5. Spatial Interpolation Method

For investigating the spatial patterns of ET_{ref} and their trends, some spatial interpolation methods, such as spline, ordinary kriging (OK), and the inverse distance weighted (IDW), were implemented on account of datasets of meteorological stations being widely employed recently. Among these interpolation approaches, the IDW approach was adopted for the spatial pattern analysis in our study since it provides the lower mean error than the others [60,61]. The main justification for using the IDW technique is that it computes the spatially-interpolated values very quickly and accurately. All spatial distribution maps were prepared using the ArcGIS (version 9.3) software (Environmental Systems Research Institute (ESRI), Redlands, CA, USA).

2.6. Sensitivity Coefficient Estimation

For identifying sensitivities of ET_{ref} to meteorological factors, the differential method proposed by McCuen [27] is applied for this study

$$S(v_i) = \lim_{\Delta v_i/v_i} \left(\frac{\Delta ET_{ref}/ET_{ref}}{\Delta v_i/v_i} \right) = \frac{\partial ET_{ref}}{\partial v_i} \times \frac{v_i}{ET_{ref}} \quad (9)$$

where $S(v_i)$ refers to the sensitivity coefficient of ET_{ref} in relation to climatic variables (v_i). The positive (negative) sensitivities illustrate the ET_{ref} increases (decreases) are accompanied with the increases in v_i . The absolute value of $S(v_i)$ represents the effect of a given v_i on ET_{ref} . The specific derived calculation formula can be found from other literature [16].

2.7. Contributions of Climate Factors on ET_{ref}

The differential equation method indicates that the ET_{ref} is the function of meteorological variables. In previous studies [40,43], four meteorological variables (mean temperature (TA , °C), actual vapor pressure (e_a , kPa), wind speed at two-meter height (WS , $m \cdot s^{-1}$), solar radiation (SR , $MJ \cdot m^{-2} \cdot day^{-1}$)) were selected as main influence factors to ET_{ref} , however, e_a was not an independent variable, but a dependent variable function of TA and relative humidity (RH , %), considering the independence of each meteorological variable, we decided to replace the e_a by RH in this study. Thus, the improved the differential equation method was used to estimate the individual contribution of each climate factor (TA , RH , WS , and SR) to ET_{ref} change trend based on the FAO-56 PM model. The detailed differential equation is

$$\frac{dET_{ref}}{dt} = \frac{\partial ET_{ref}}{\partial TA} \frac{dTA}{dt} + \frac{\partial ET_{ref}}{\partial RH} \frac{dRH}{dt} + \frac{\partial ET_{ref}}{\partial WS} \frac{dWS}{dt} + \frac{\partial ET_{ref}}{\partial SR} \frac{dSR}{dt} + \varepsilon \quad (10)$$

or, written briefly,

$$C_{ET_{ref}} = C(TA) + C(RH) + C(WS) + C(SR) + \varepsilon \quad (11)$$

where $C_{ET_{ref}}$ refers to long term estimated trend of ET_{ref} , $C(TA)$, $C(RH)$, $C(WS)$, and $C(SR)$ are contributions to ET_{ref} due to changes in TA , RH , WS , and SR , respectively. ε refers to the error term between the $C_{ET_{ref}}$ and ET_{ref} trends estimated by Theil-Sen's estimator ($T_{ET_{ref}}$). The contribution of each selected climate factor to the ET_{ref} trend can be obtained by calculating the averaged partial derivatives (Equations (9) and (10)) multiplied by the annual/seasonal tendency rates and the length of time (namely 365 or 366 for annual, 214 for growing season, 92 for spring and summer, 91 for autumn, and 90 or 91 for winter).

3. Results

3.1. Variations of Climate Factors and Their Trend Analysis

Variations of monthly climate factors are shown in Figure 2. From Figure 2, monthly *TA* and *SR* exhibited similar variation patterns. The peak value occurred in June and July. The largest regional differences of *SR* were shown in spring and summer seasons, while the largest regional difference of *TA* exhibited in winter. Meanwhile, *RH* gradually increased before August and then decreased. Monthly *WS* values represent a fluctuating variation trend, the peak and valley values occurred in April and September, respectively.

The effects evaluation of climate factors to ET_{ref} was implemented by analyzing temporal trends of four meteorological parameters from 1961 to 2014 in the HRB. As from Figure 3, *TA* showed an overall upward trend in the past 54 years. It was noteworthy that a slow decreasing trend was observed before the 1990s and then a significantly increasing trend was observed. The *RH* fluctuated obviously, with a non-significant declining trend in the whole HRB. The *WS* and *SR* exhibited more significant declining trends in comparison with *TA* and *RH*.

The similar results can also be detected from Table 1. At the seasonal time scale, *TA* revealed a significant increasing trend in each season except the summer. Opposite to *TA*, *RH* exhibited a reverse change trend. Meanwhile, significant decreasing *RH* trends were found in the lower HRB in each season compared to the other regions. *WS* always exhibited a significant downward trend in all regions at each time scale, which could also be verified from Figure 3. The *SR* revealed a significant decreasing trend in the whole HRB in all time periods except spring.

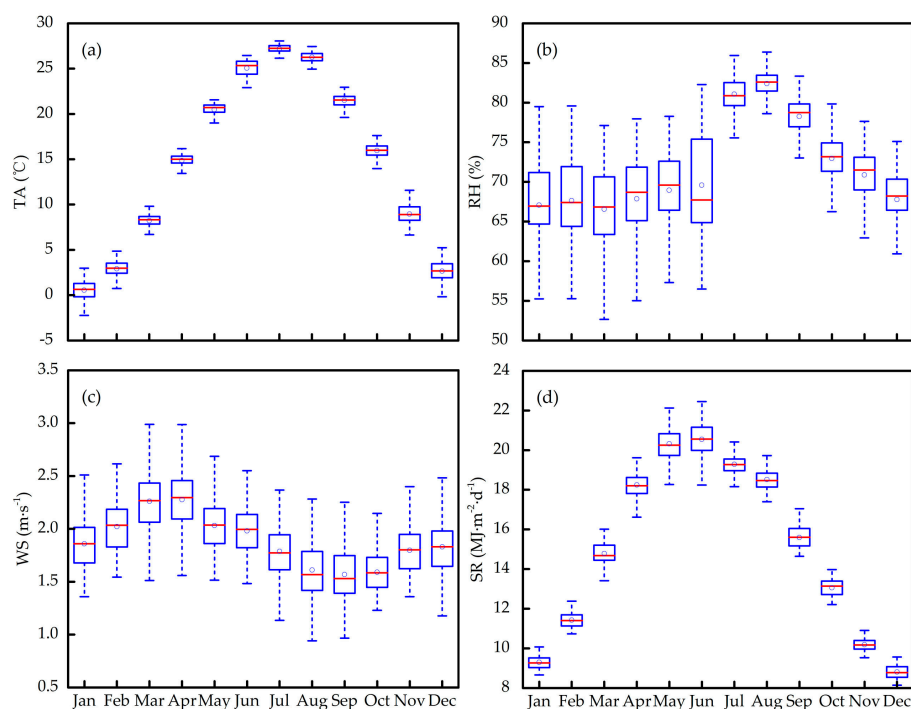


Figure 2. Box plots show the monthly variations of (a) *TA*; (b) *RH*; (c) *WS*; and (d) *SR* in the HRB.

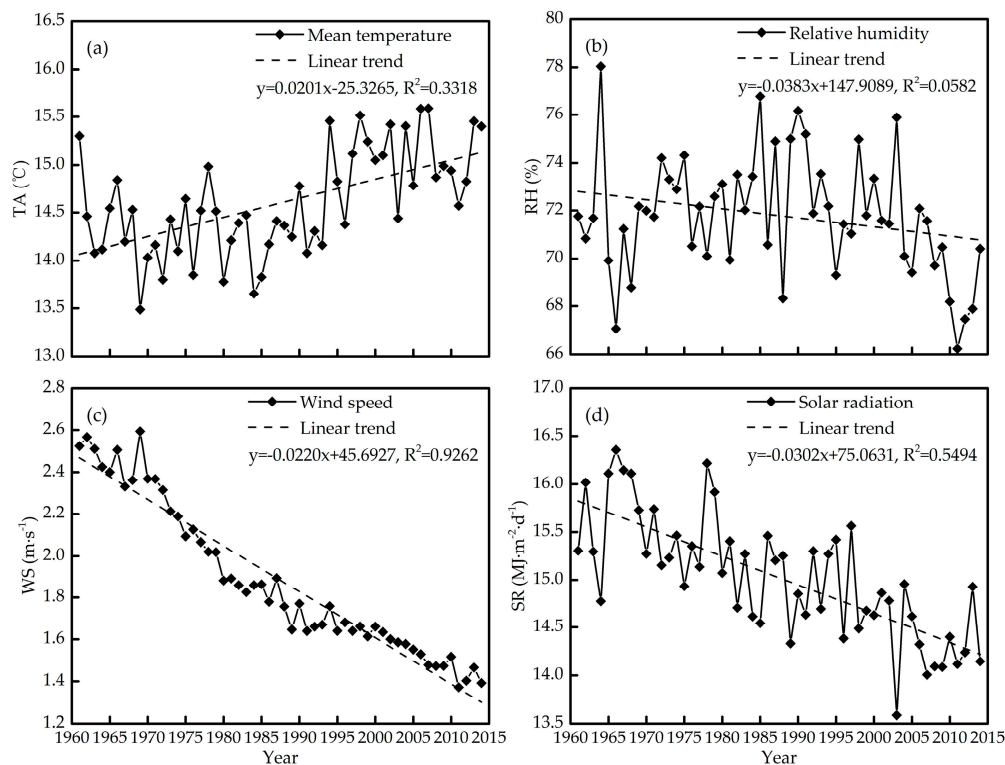


Figure 3. Temporal trends of (a) TA; (b) RH; (c) WS; and (d) SR in the HRB during 1961–2014.

3.2. Variations of ET_{ref} and Their Trend Analysis

In order to obtain insights into the spatial distributions of annual and seasonal ET_{ref} in the HRB, the annual averaged ET_{ref} in each station from 1961 to 2014 was spatially interpolated using the IDW method (Figure 4). The annual ET_{ref} during the past 54 years in the HRB ranged from 881 mm to 1091 mm, with an average value of 969.56 mm. The higher values were observed in the north of the middle and Yi-Shu-Si River basins. Similar spatial distributions of ET_{ref} were identified during the growing season and spring, ranging from 689 mm to 863 mm, and from 245 mm to 345 mm, respectively. Meanwhile, the lower values of ET_{ref} mainly distributed in the upper and lower HRB. However, in the summer, the ET_{ref} was much higher than other seasons (336–427 mm), and the higher ET_{ref} values expanded to most parts of the upper and middle HRB also the Yi-Shu-Si River Basin. In autumn and winter, differences of ET_{ref} were smaller in the whole HRB. The higher values were observed in the southeast in autumn, and in the northwest in winter. In general, the ET_{ref} demonstrated a strong spatial heterogeneity in the whole HRB.

Table 1. Seasonal and annual trend analyses of climatic factors in each region of the HRB during 1961–2014.

Region	Climatic Factor	Annual		Growing Season		Spring		Summer		Autumn		Winter	
		Z	β	Z	β	Z	β	Z	β	Z	β	Z	β
Upper	TA (°C)	3.48	0.01 ***	2.18	0.010 *	3.76	0.034 ***	−0.91	−0.007	2.51	0.015 *	2.76	0.025 **
	RH (%)	−1.55	−0.035	−0.79	−0.027	−2.81	−0.133 **	2.09	0.056 *	−1.79	−0.065	−0.85	−0.051
	WS (m·s ^{−1})	−9.37	−0.019 ***	−9.13	−0.019 ***	−8.30	−0.020 ***	−8.16	−0.019 ***	−8.31	−0.020 ***	−8.18	−0.020 ***
	SR (MJ·m ^{−2} ·day ^{−1})	−5.09	−0.030 ***	−4.36	−0.038 ***	−0.39	−0.005	−5.13	−0.062 ***	−2.27	−0.018 *	−3.52	−0.023 ***
Middle	TA (°C)	3.57	0.018 ***	2.04	0.010 *	3.57	0.030 ***	−0.60	−0.004	3.18	0.016 **	3.49	0.032 ***
	RH (%)	−0.55	−0.015	−0.13	−0.005	−1.33	−0.064	1.39	0.040	−1.61	−0.061	−0.64	−0.039
	WS (m·s ^{−1})	−9.71	−0.022 ***	−9.58	−0.021 ***	−9.04	−0.024 ***	−9.09	−0.020 ***	−8.94	−0.021 ***	−8.56	−0.023 ***
	SR (MJ·m ^{−2} ·day ^{−1})	−6.01	−0.035 ***	−5.42	−0.045 ***	−1.09	−0.012	−5.82	−0.072 ***	−3.10	−0.026 ***	−4.15	−0.029 ***
Yi-Shu-Si	TA (°C)	4.86	0.025 ***	3.63	0.017 ***	4.46	0.035 ***	1.03	0.006	3.67	0.021 ***	4.43	0.040 ***
	RH (%)	−1.79	−0.042	−1.60	−0.035	−1.66	−0.075	−0.57	−0.012	−1.31	−0.050	−1.01	−0.053
	WS (m·s ^{−1})	−8.97	−0.021 ***	−8.85	−0.021 ***	−8.55	−0.025 ***	−8.46	−0.019 ***	−7.80	−0.019 ***	−7.58	−0.020 ***
	SR (MJ·m ^{−2} ·day ^{−1})	−5.82	−0.030 ***	−5.18	−0.038 ***	−1.34	−0.010	−5.82	−0.062 ***	−3.27	−0.025 **	−3.83	−0.023 ***
Lower	TA (°C)	4.67	0.027 ***	3.88	0.023 ***	4.79	0.039 ***	1.31	0.012	4.07	0.026 ***	3.89	0.034 ***
	RH (%)	−4.79	−0.109 ***	−4.74	−0.120 ***	−4.01	−0.178 ***	−3.36	−0.085 ***	−3.60	−0.107 ***	−2.95	−0.098 **
	WS (m·s ^{−1})	−8.76	−0.021 ***	−8.27	−0.019 ***	−8.58	−0.025 ***	−7.46	−0.017 ***	−7.33	−0.019 ***	−7.88	−0.022 ***
	SR (MJ·m ^{−2} ·day ^{−1})	−4.10	−0.018 ***	−3.27	−0.023 **	0.95	0.009	−4.18	−0.056 ***	−1.45	−0.009	−2.42	−0.017 *
Whole	TA (°C)	4.06	0.021 ***	2.78	0.013 **	3.88	0.032 ***	0.10	0.001	3.52	0.018 ***	3.77	0.035 ***
	RH (%)	−1.64	−0.038	−1.28	−0.028	−1.76	−0.083	0.18	0.005	−1.87	−0.062	−0.97	−0.054
	WS (m·s ^{−1})	−9.64	−0.021 ***	−9.50	−0.020 ***	−8.98	−0.024 ***	−9.00	−0.019 ***	−8.64	−0.020 ***	−8.40	−0.022 ***
	SR (MJ·m ^{−2} ·day ^{−1})	−5.73	−0.030 ***	−5.25	−0.040 ***	−0.72	−0.007	−5.79	−0.066 ***	−3.07	−0.022 **	−3.80	−0.025 ***

Note: *, **, and *** denote the significance levels of 0.05, 0.01, and 0.001, respectively. β is the estimated slope trend of ET_{ref} , $\beta > 0$ and $\beta < 0$ signify an upward and a downward trend, respectively. Z is the Mann–Kendall test statistic.

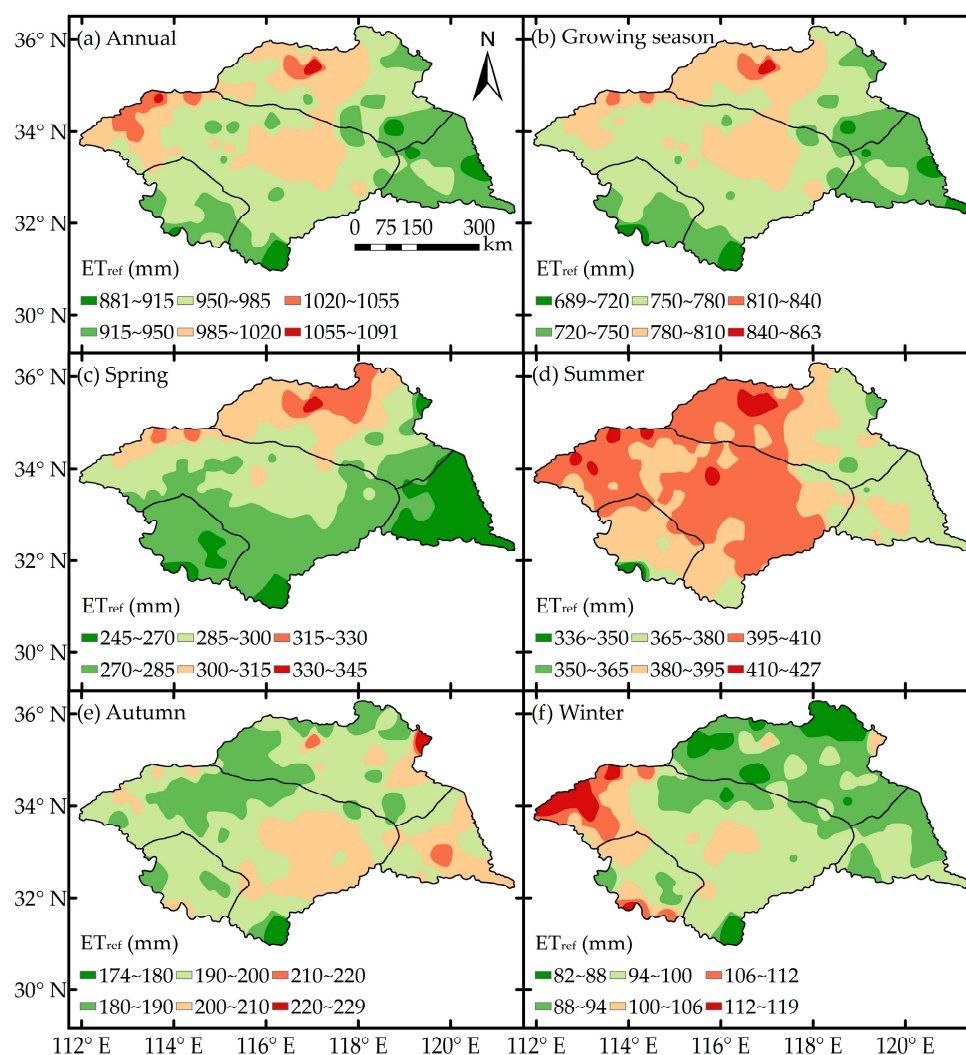


Figure 4. Spatial distribution maps of (a) annual; (b) growing season; (c) spring; (d) summer; (e) autumn; and (f) winter ET_{ref} during 1961–2014 in the HRB.

As shown in Table 2, at the annual time scale, a significant downward trend of ET_{ref} was found in the whole HRB ($-1.894 \text{ mm}\cdot\text{a}^{-2}$), the upper and middle HRB and the Yi-Shu-Si River Basin. A non-significant upward trend was detected in the lower HRB ($0.177 \text{ mm}\cdot\text{a}^{-2}$). The magnitude of the ET_{ref} trend followed the order: Middle > Upper > Yi-Shu-Si > Lower. During the growing season, the magnitude of the change rate was slightly lower than that at the annual time scale, while the spatial distribution was similar to that of the annual time scale. At the seasonal time scale, the magnitude of the change rates of ET_{ref} ranked in sequence as: summer > autumn > spring > winter in most of the HRB, except the lower HRB, while in the lower HRB the magnitude of change rates of ET_{ref} ranked in a sequence as: spring > summer > autumn > winter. In spring, only ET_{ref} in the lower HRB exhibited a significant increasing trend. In summer, ET_{ref} in all sub-regions showed significant decreasing trends. In autumn, ET_{ref} in the middle HRB and Yi-Shu-Si River Basin exhibited significant decreasing trends. However, in winter, no sub-region showed significant change trends. In the whole region, significant decreasing trends were observed at most time scales, except spring and winter, during which the change rate of ET_{ref} was the largest in the annual time scale.

The spatial distribution of seasonal ET_{ref} trends is displayed in Figure 5. Similar spatial distribution (increased from northwest to southeast) was observed at the annual time scale and during the growing season, ranging from $-4.87 \text{ mm}\cdot\text{a}^{-2}$ to $1.79 \text{ mm}\cdot\text{a}^{-2}$ and $-4.38 \text{ mm}\cdot\text{a}^{-2}$ to $1.28 \text{ mm}\cdot\text{a}^{-2}$,

respectively. Among which, most decreasing trends were significant. In spring, the significant downward ET_{ref} trends were detected in the north parts of middle HRB and Yi-Shu-Si River Basin stations. However, ET_{ref} in the majority of stations of the lower HRB exhibited significant upward trends. Similar significant increasing trends could also be detected in some stations in the southern upper and middle HRB. In summer, more than 90% of stations demonstrated the significant decreasing trends of ET_{ref} , except the lower HRB. A general downward trend in ET_{ref} was observed in autumn and winter, with about 52% and 26% of stations exhibiting significant decreasing trends, respectively.

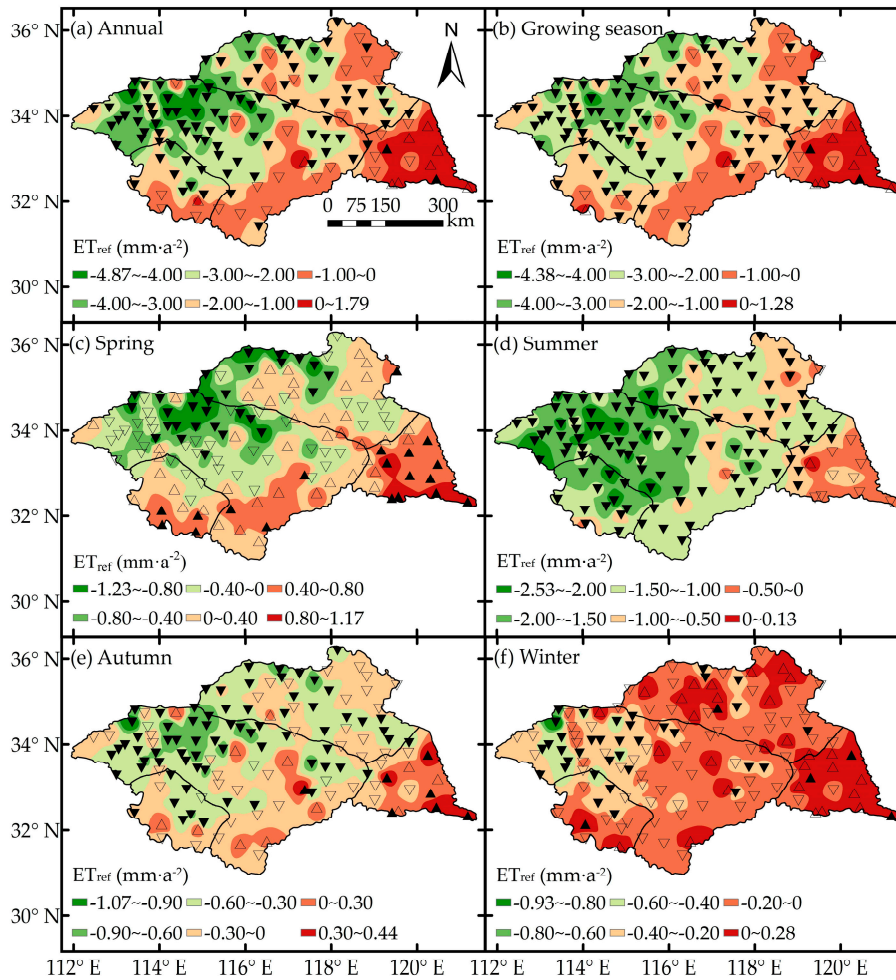


Figure 5. Spatial distribution maps of (a) annual; (b) growing season; (c) spring; (d) summer; (e) autumn; and (f) winter ET_{ref} trends during 1961–2014 in the HRB. The upward and downward triangles represent increasing and decreasing ET_{ref} trends. The solid black triangle represents a significance level of 0.05.

Table 2. Seasonal and annual trends of ET_{ref} ($\text{mm}\cdot\text{a}^{-2}$) during 1961–2014 in each region of the HRB.

Region	Annual		Growing Season		Spring		Summer		Autumn		Winter	
	Z	β	Z	β	Z	β	Z	β	Z	β	Z	β
Upper	−3.49	−1.787 ***	−3.55	−1.578 ***	0.69	0.197	−4.97	−1.567 ***	−1.76	−0.253	−1.12	−0.138
Middle	−4.74	−2.561 ***	−4.92	−2.287 ***	−1.06	−0.331	−5.43	−1.596 ***	−2.73	−0.400 **	−1.82	−0.235
Yi-Shu-Si	−3.88	−1.556 ***	−3.83	−1.446 ***	−0.60	−0.153	−4.43	−1.094 ***	−2.25	−0.276 *	−0.39	−0.044
Lower	0.45	0.177	0.15	0.062	3.04	0.660 **	−1.97	−0.498 *	0.91	0.100	0.93	0.075
Whole	−4.09	−1.894 ***	−4.25	−1.772 ***	−0.39	−0.122	−4.64	−1.307 ***	−2.40	−0.308 *	−1.24	−0.143

Note: *, **, and *** denote the significance levels of 0.05, 0.01, and 0.001, respectively. β refers to the estimated slope trend of ET_{ref} , $\beta > 0$ and $\beta < 0$ signify an upward and a downward trend, respectively. Z is the Mann–Kendall test statistic.

3.3. Sensitivity Coefficient of ET_{ref} to Climate Factors

To explore the effects of climate factors on ET_{ref} , sensitivity coefficients of air temperature, relative humidity, wind speed, and solar radiation in each time period of the HRB are shown in Table 3. Among all climate factors, only the RH showed negative sensitivity coefficients. Moreover, it declared that the ET_{ref} showed more sensitivity to RH , with SR , TA , and WS followed closely at the annual time scale in the whole HRB and every sub-region. In growing season, ET_{ref} in the upper and lower HRB showed the highest sensitivity to RH , while the whole HRB and other sub-regions showed the highest sensitivity to SR . At seasonal time scales, RH was the most sensitive factor in the whole HRB and all sub-regions except in summer. However, in summer, SR was the most sensitive factor in the whole HRB and most sub-regions, except the lower HRB. Meanwhile, RH was still the most sensitive factor in the lower HRB. In addition, the sensitivities of ET_{ref} to TA and SR were higher in the summer and during the growing season, but lower in the winter. The sensitivities of ET_{ref} to RH in autumn and winter seasons were much greater than that of other seasons. A detailed spatial distribution of sensitivity coefficients in each time period can be found in Figure 6.

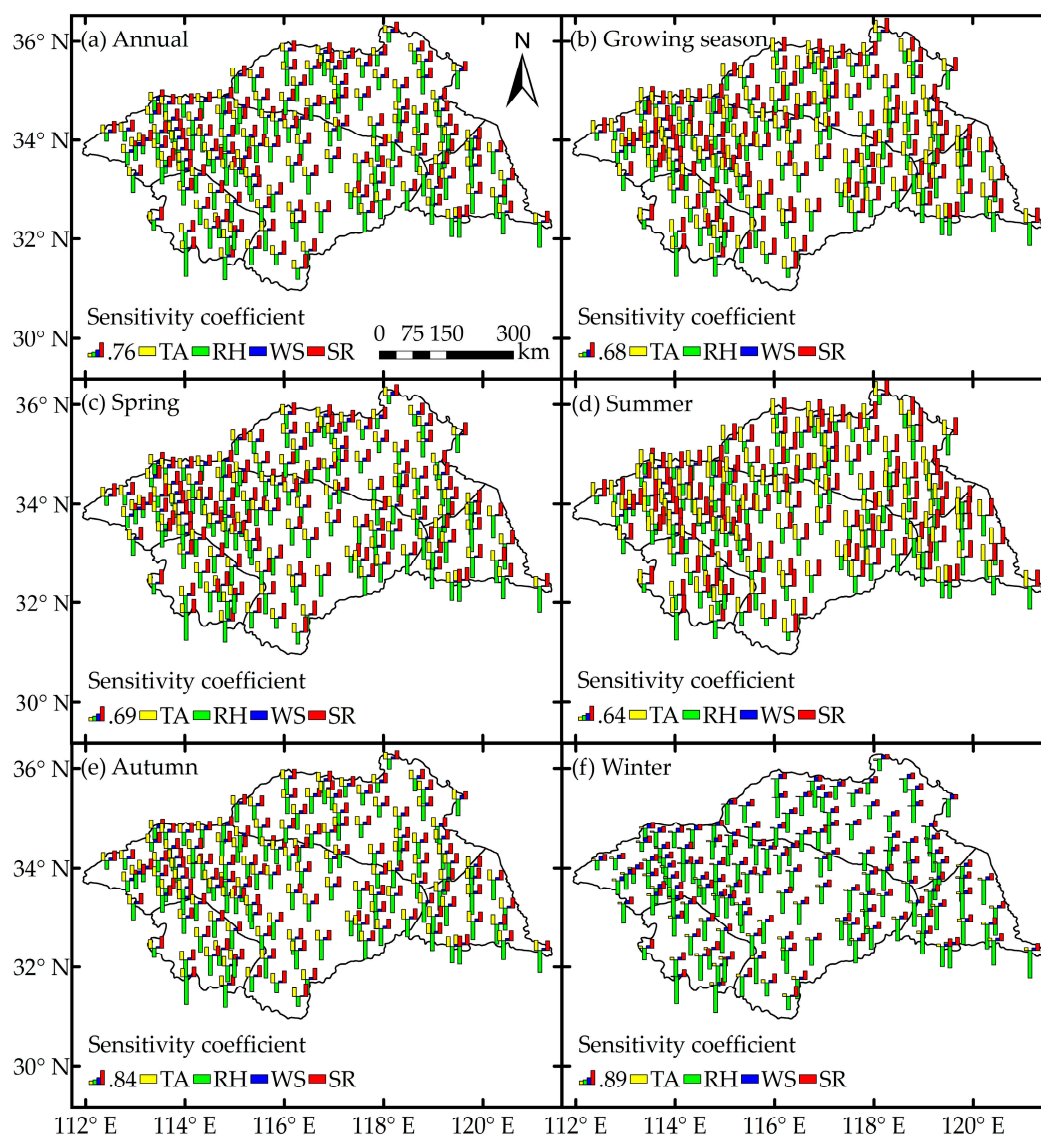


Figure 6. Spatial distribution maps of (a) annual; (b) growing season; (c) spring; (d) summer; (e) autumn; and (f) winter sensitivity coefficients during 1961–2014 in the HRB.

Table 3. Annual and seasonal sensitivity coefficients of ET_{ref} to the main climate factors in each region of the HRB during 1961–2014.

Region	Sensitivity Coefficient	Annual	Growing Season	Spring	Summer	Autumn	Winter
Upper	$S(TA)$	0.463	0.634	0.493	0.695	0.541	0.122
	$S(RH)$	−0.963	−0.764	−0.853	−0.675	−1.032	−1.301
	$S(WS)$	0.115	0.077	0.089	0.055	0.131	0.184
	$S(SR)$	0.642	0.737	0.666	0.793	0.630	0.480
Middle	$S(TA)$	0.461	0.640	0.498	0.700	0.544	0.102
	$S(RH)$	−0.850	−0.669	−0.739	−0.597	−0.907	−1.165
	$S(WS)$	0.140	0.095	0.114	0.073	0.152	0.222
	$S(SR)$	0.615	0.720	0.637	0.779	0.609	0.436
Yi-Shu-Si	$S(TA)$	0.436	0.639	0.480	0.699	0.536	0.028
	$S(RH)$	−0.813	−0.663	−0.678	−0.642	−0.852	−1.082
	$S(WS)$	0.156	0.100	0.138	0.065	0.169	0.253
	$S(SR)$	0.582	0.701	0.591	0.778	0.577	0.383
Lower	$S(TA)$	0.481	0.662	0.488	0.724	0.588	0.122
	$S(RH)$	−1.128	−0.929	−1.037	−0.864	−1.135	−1.478
	$S(WS)$	0.111	0.067	0.074	0.042	0.138	0.191
	$S(SR)$	0.614	0.718	0.636	0.783	0.602	0.433
Whole	$S(TA)$	0.459	0.643	0.493	0.703	0.549	0.091
	$S(RH)$	−0.892	−0.713	−0.777	−0.653	−0.939	−1.204
	$S(WS)$	0.138	0.090	0.112	0.065	0.152	0.222
	$S(SR)$	0.610	0.717	0.629	0.781	0.602	0.427

Note: The bold fonts represent the most sensitive factors in each time period.

3.4. Quantitative Contributions of Climate Factors to ET_{ref}

The contributions from climate factors to the long-term ET_{ref} change trends were calculated by Equation (10). As observed from Figure 7, the change trends of the annual and seasonal ET_{ref} estimated using Equation (10) ($C_{ET_{ref}}$) were well fitted with ET_{ref} trends estimated by the Theil–Sen’s estimator ($T_{ET_{ref}}$). The R-squared value was larger than 0.94 in each time period and the slopes of the linear fit approximated to 1. The specific ET_{ref} change trends calculated from two approaches in all sub-regions in all time scales can be found in Table 4. The well-fitted relationship between $C_{ET_{ref}}$ and $T_{ET_{ref}}$ suggested that it was reasonable and reliable to adopt the four climate factors in Equation (10) to estimate its contributions to the change trends in ET_{ref} .

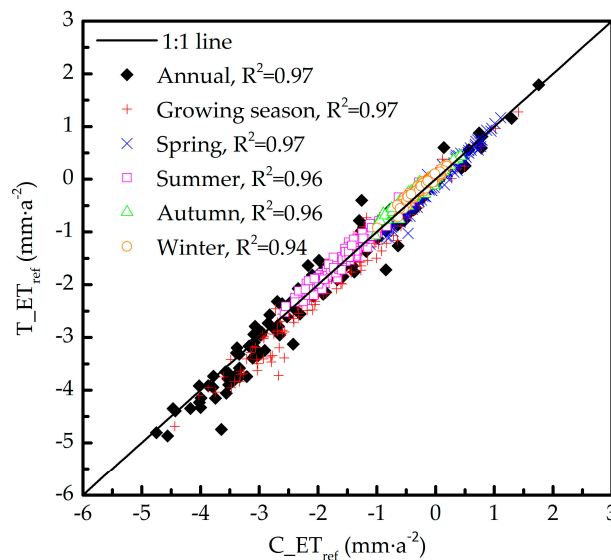


Figure 7. Relationship between the calculated $C_{ET_{ref}}$ and the estimated ET_{ref} trend ($T_{ET_{ref}}$) by Theil–Sen’s estimator.

Based on the accuracy and applicability of the modified differential equation method, as shown from Table 4, TA and RH had positive contributions to ET_{ref} in the whole HRB and all sub-regions,

except in some regions in summer. During the summer, *TA* showed small negative contributions in the upper and middle HRB, and *RH* showed small negative contributions in the whole HRB, upper, and middle HRB. *WS* and *SR* had negative contributions in the whole HRB and all sub-regions, except small positive contributions in the lower HRB in spring. This demonstrated that *TA* and *RH* were mainly responsible for the increasing trend in ET_{ref} , while *WS* and *SR* were mainly responsible for the decreasing trend in ET_{ref} . At an annual time scale, with spring, autumn and winter, *WS* contributed the most to ET_{ref} trends in the whole HRB and most sub-regions, except the lower HRB. In growing season and summer, *SR* contributed the most to ET_{ref} trends in the whole HRB and most sub-regions except the lower HRB. However, in the lower HRB, these factors contributed differently from other regions. The most contributive factor was *RH* at the annual time scale, growing season and in spring, then turned to *SR* in the summer and to *WS* in the autumn and winter. Further, it was noteworthy that positive contributions of *TA* and *RH* could not counteract the negative ones of *WS* and *SR*, which generated a significant downward trend ($-1.894 \text{ mm}\cdot\text{a}^{-2}$) in the entire HRB at the annual time scale. Overall, this implies that the significant decrease of *WS* was the dominant contributing factor in ET_{ref} decline, followed by *SR*, *TA*, and *RH*, respectively. Similar findings were found in the upper, middle HRB and Yi-Shu-Si River Basin. Additionally, at seasonal time scales, the total contributions of the climatic variables in growing season and summer were much greater than that of the contributions in spring, autumn and winter seasons, which fit reasonably well with results from Table 1. Although the ET_{ref} was most sensitive to *RH*, the contribution of *RH* to ET_{ref} was generally less in the whole region. On the other hand, the ET_{ref} was the least sensitive to *WS* but the contribution of *WS* was the highest in the study area. Furthermore, the most vital contributing factor *RH* in the growing season and spring in the lower HRB merited more attention.

Table 4. Annual and seasonal contributions ($\text{mm}\cdot\text{a}^{-2}$) of the main climate factors to ET_{ref} in each region of the HRB during 1961–2014.

Region	Contribution	Annual	Growing Season	Spring	Summer	Autumn	Winter
Upper	<i>C(TA)</i>	0.572	0.248	0.324	-0.056	0.103	0.133
	<i>C(RH)</i>	0.236	0.111	0.296	-0.153	0.121	0.066
	<i>C(WS)</i>	-1.300	-0.775	-0.334	-0.281	-0.386	-0.289
	<i>C(SR)</i>	-1.217	-1.203	-0.057	-1.028	-0.191	-0.122
	<i>C_ET_{ref}</i>	-1.710	-1.619	0.228	-1.517	-0.353	-0.211
	<i>T_ET_{ref}</i>	-1.787	-1.578	0.197	-1.567	-0.253	-0.138
	Middle	<i>C(TA)</i>	0.584	0.225	0.297	-0.039	0.121
<i>C(RH)</i>		0.054	0.008	0.141	-0.123	0.105	0.047
<i>C(WS)</i>		-1.777	-1.038	-0.488	-0.405	-0.446	-0.389
<i>C(SR)</i>		-1.383	-1.358	-0.115	-1.123	-0.257	-0.125
<i>C_ET_{ref}</i>		-2.523	-2.163	-0.166	-1.690	-0.476	-0.309
<i>T_ET_{ref}</i>		-2.561	-2.287	-0.331	-1.596	-0.400	-0.235
Yi-Shu-Si		<i>C(TA)</i>	0.831	0.417	0.375	0.065	0.159
	<i>C(RH)</i>	0.289	0.153	0.177	0.020	0.092	0.078
	<i>C(WS)</i>	-1.622	-0.977	-0.567	-0.321	-0.395	-0.325
	<i>C(SR)</i>	-1.133	-1.130	-0.096	-0.986	-0.224	-0.087
	<i>C_ET_{ref}</i>	-1.635	-1.537	-0.112	-1.223	-0.368	-0.134
	<i>T_ET_{ref}</i>	-1.556	-1.446	-0.153	-1.094	-0.276	-0.044
	Lower	<i>C(TA)</i>	0.878	0.523	0.379	0.119	0.189
<i>C(RH)</i>		1.012	0.768	0.467	0.242	0.243	0.154
<i>C(WS)</i>		-0.983	-0.540	-0.285	-0.157	-0.285	-0.241
<i>C(SR)</i>		-0.753	-0.720	0.056	-0.869	-0.109	-0.069
<i>C_ET_{ref}</i>		0.155	0.031	0.617	-0.665	0.039	0.012
<i>T_ET_{ref}</i>		0.177	0.062	0.660	-0.498	0.100	0.075
Whole		<i>C(TA)</i>	0.679	0.310	0.329	0.004	0.137
	<i>C(RH)</i>	0.254	0.151	0.207	-0.046	0.122	0.071
	<i>C(WS)</i>	-1.608	-0.944	-0.473	-0.345	-0.411	-0.347
	<i>C(SR)</i>	-1.222	-1.204	-0.080	-1.047	-0.223	-0.108
	<i>C_ET_{ref}</i>	-1.897	-1.687	-0.018	-1.434	-0.374	-0.217
	<i>T_ET_{ref}</i>	-1.894	-1.772	-0.122	-1.307	-0.308	-0.143

Note: The bold fonts represent the most contributing factor in each time period.

Figure 8 exhibits the seasonal and annual contributions of four climate factors to long-term ET_{ref} change trends in each meteorological station in the study period. WS was the dominate driving force to the changes in ET_{ref} at the annual time scale and spring, autumn, and winter seasons, which occupied 93, 94, 109, and 122 stations among a total of 137 stations in the whole HRB, respectively. On the contrary, in the same time scales, TA , RH , and SR were the dominate driving force to the changes in ET_{ref} , occupied 6, 6, 32 stations; 21, 21, 1 stations; 3, 8, 17 stations; and 10, 1, 4 stations among a total of 137 stations in the HRB, respectively. In the growing season and summer, SR contributed most to the change trends of ET_{ref} , especially in summer, which played a dominant role and occupied about 98.5% of stations of the entire HRB. Meanwhile, the TA , RH , WS , and SR acted as dominant parts in the changes of ET_{ref} at 1, 9, 45, and 82 stations during the growing season, respectively.

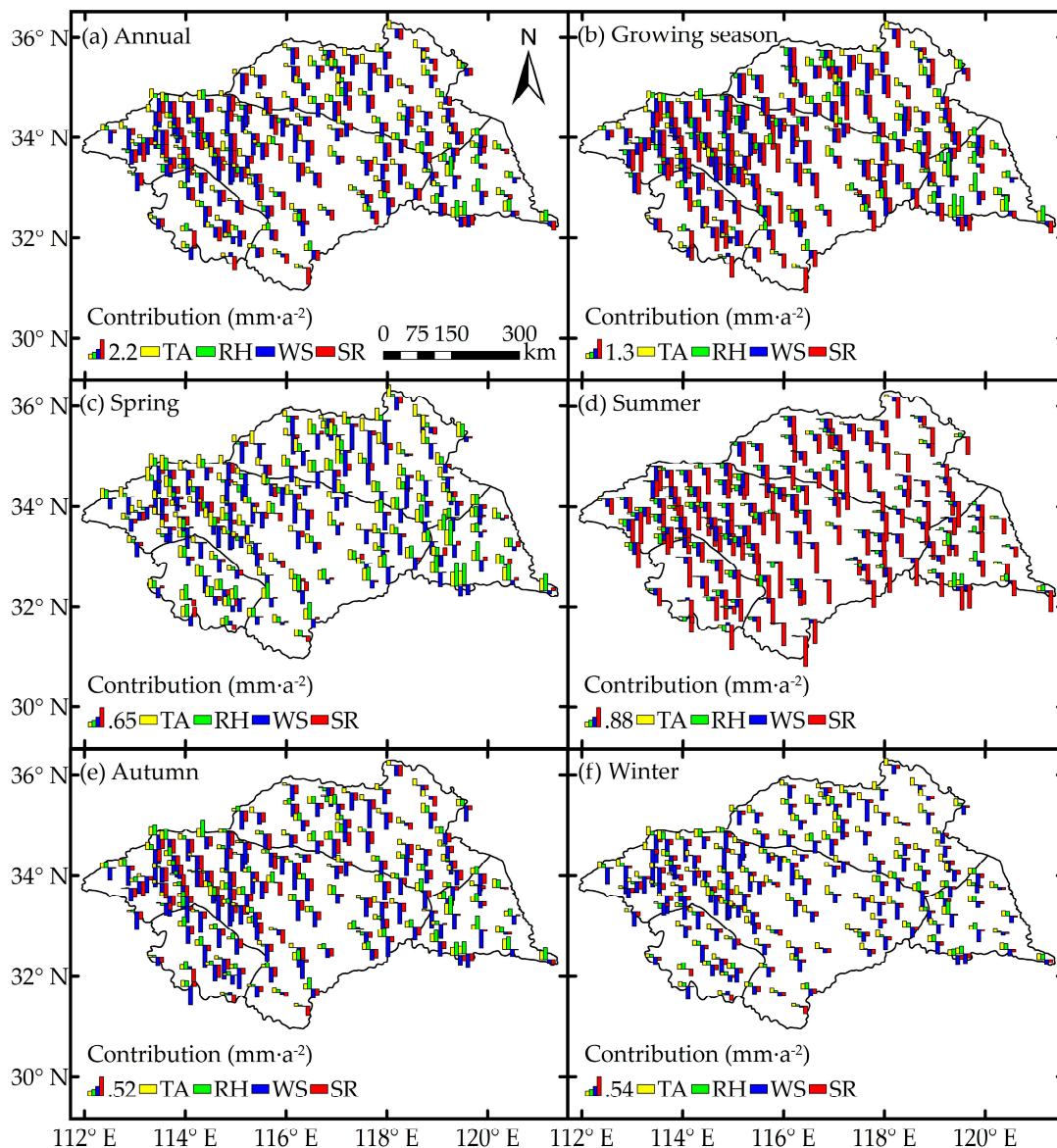


Figure 8. Spatial distribution patterns of contributions of climate factors to ET_{ref} in (a) annual; (b) growing season; (c) spring; (d) summer; (e) autumn; and (f) winter during 1961–2014 in the HRB.

4. Discussion

4.1. Temporal Change Trends of ET_{ref} and Climate Factors in HRB

Global warming has become an accepted fact in the present era [31]. The warming rate in the global mean surface temperature from 1951 to 2012 was $0.012\text{ }^{\circ}\text{C}\cdot\text{a}^{-1}$. However, the significant increasing rate in TA ($0.021\text{ }^{\circ}\text{C}\cdot\text{a}^{-1}$) in the entire HRB was two-fold larger than the global average [7], which was echoed by Sun et al. [62]. An interesting phenomenon was observed in this study that the TA in the upper and middle HRB demonstrated a slow and non-significant decreasing trend in summer.

Recently, the most significant decreasing rate of WS ($-0.021\text{ m}\cdot\text{s}^{-1}\cdot\text{a}^{-1}$) was detected in each time scale in the HRB. Similar results were also found elsewhere [63]. The decreasing WS rate agreed well with result of Guo et al. [64]. However, the magnitude of decreasing rate of WS in the HRB was much greater than those in the other river basins [1,21] and different areas in China [65,66], and also in East Asia [67]. The recent declining WS trend is mostly a result of large-scale atmospheric circulation patterns on account of climate warming [68], weakened Siberian High and East Asia Monsoon [69], descending temperature and pressure gradient [69–71], and intensified Asian zonal circulation patterns [72]. In addition, increased land surface roughness caused by the increased vegetation cover can give a reasonable explanation for the decreasing WS trend. Shan et al. [33] also found this was the reason for declining of WS rate, especially in Northwest China, where Chinese forestry and ecological projects have been implemented in large-scale forestation and reforestation. Furthermore, accelerated urbanization caused by population expansion and economic growth may be reasons for decreased WS , particularly in the regions near weather stations. Additionally, the decreasing WS will reduce the migration of water molecules, reducing the impact of aerodynamic force on ET_{ref} , therefore, lead to a downward trend in ET_{ref} [73]. However, the significant downward trend in the WS at each station of the HRB is still a debatable matter and needs further study.

Solar radiation (SR) as one crucial energy source, has found to be in a decreasing trend [1,21,43] which is similar to our results in the HRB. The radiation observation data showed that the SR decreased before 1980s [74,75], then gradually increased after 1990s, this phenomenon was named “from dimming to brightening” by Wild et al. [76]. As seen from Figure 3d, this phenomenon is not obvious in the HRB, and SR exhibited a significant downward trend at the rate of $-0.03\text{ MJ}\cdot\text{m}^{-2}\cdot\text{day}^{-1}\cdot\text{a}^{-1}$ in the annual time scale in the whole HRB. Possible reasons for this decreasing tendency are (1) the increased regional cloud cover [77]; (2) the increased aerosol loading due to the pollutants from anthropogenic emission [78,79]; (3) increased atmospheric moisture and the aggravated air-pollution caused by the energy depletion; and (4) the significant decreasing WS rate which restrained the spread of aerosols and pollutants [80].

In this study, we have drawn a conclusion that the TA increased significantly with a rate of $0.021\text{ }^{\circ}\text{C}\cdot\text{a}^{-1}$ in last 54 years in the HRB, whereas, the ET_{ref} exhibited a significant downward trend ($-1.894\text{ mm}\cdot\text{a}^{-2}$) in the whole region. The significant decreasing ET_{ref} in the HRB is in disagreement with climate warming result [81,82]. This differs from the earlier findings by Hulme et al. [83] and Goyal [82]. In fact, the two adverse change trends between the TA and ET_{ref} are titled the “evaporation paradox” proposed by Brutsaert and Parlange [13]. This paradoxical situation occurred in the HRB, especially in the upper and lower HRB and the Yi-Shu-Si River Basin. This finding is echoed with similar works in major basins of the Yangtze River [1], lower Yellow River [21], and Haihe River [84] in China and in many regions worldwide [5,11,85]. However, our results about the “evaporation paradox” slightly differ from the outcomes proposed by Thomas [15] which showed an increasing trend of ET_{ref} in the northeast and southwest region of China. This is because of the absence of a long-term meteorological dataset, a shortage of weather stations, and different study periods and areas in his research; whereas our study data source is a long-time series dataset (1961–2014) from 137 weather stations. McVicar et al. [63] conducted a worldwide research to study the ET_{ref} trend in the last three decades, then the downward tendency was detected in many parts worldwide. However, the lower HRB demonstrated an increasing ET_{ref} , this is also proved by results from Chu et al. [16].

4.2. Impact of Climate Factors to ET_{ref} Trends

The outcomes exhibited that the RH was the most sensitive factor of ET_{ref} in HRB, followed by SR , TA , and WS , respectively, which coincided with the conclusions proposed by Gong et al. [86] and Li et al. [31] in the Yangtze River Basin and also the Loess Plateau of Northern Shaanxi, China. However, in summer and during the growing season, the ET_{ref} showed the most sensitivity to SR , with TA , RH , and WS following, respectively. Similar findings could also be found in Spain [87] and the United States [88]. Additionally, the RH was the most sensitive factor in ET_{ref} in each time period of the lower HRB. All these discoveries are in accordance with the findings from Chu et al. [16] in Jiangsu Province, Eastern China. In fact, the meteorological factors influence ET_{ref} differently in different study areas. Huo et al. [14] indicated that the WS had the strongest sensitivity in arid Northwest China. Ye et al. [32] found SD was the dominating factor, with RH , WS , and TA following in the Poyang Lake catchment. Gao et al. [30] studied the sensitivities of ET_{ref} to the climate factors in the crop growth period in West Liao River Basin, then found SR was the most sensitive factor, with RH following. Moreover, Gao et al. [35] also have demonstrated SR was the most dominant factor for ET_{ref} in the same study area at the annual time scale, but varied at the seasonal time scale. The maximum temperature (T_{max}) was the dominant climate factor for decreasing ET_{ref} in the Jing River Basin [8]. In other countries, Estévez et al. [87] proposed that ET_{ref} was most sensitive to TA , followed by RH , SR , and WS in Spain. Irmak et al. [88] found ET_{ref} was most sensitive to VPD (Vapor pressure deficit) in five locations of the United States, followed by WS in semiarid regions and SR in humid locations during the summer months. Thus, we concluded that diverse climatic conditions, different latitudes and elevations, and local environmental conditions are responsible for the various sensitivity analysis results of meteorological factors to ET_{ref} changes in various areas of the world.

In our research, we also found that WS was the dominant contributing climatic factor in the HRB. This result was echoed with results of Wang et al. [37], Zhang et al. [89], and McVicar et al. [63]. As shown above, RH was the most sensitive factor for ET_{ref} in the whole HRB, while WS was the least sensitive factor to the ET_{ref} in the same regions. This phenomenon may be due the change rate of WS was much greater than that of RH . Ultimately, WS exhibited a greater contribution to ET_{ref} trend. Thus, the higher contribution of RH in the lower HRB can be explained reasonably by the significant decreasing trend of RH in each time period shown in Table 1. However, the SR contributed more than WS in the growing season and summer, followed by TA and RH , respectively. This is mainly the result of the high values of SR concentrated in the growing season and summer (Figure 2), and its significantly decreasing trend during these periods (Table 1). Though the monthly change trend of TA was similar to SR , TA exhibited a significant increasing trend, except in summer and during the growing seasons, and these might be the main reason that SR exhibited a higher contribution to ET_{ref} than TA in the same period. However, the non-significance of the TA trend in summer and during the growing season was still unclear and needed to be further investigated. Similar to the sensitivities, the different meteorological factors contributions to ET_{ref} trends were discovered from different areas and in different climatic conditions. Fan et al. [29] reported that the ET_{ref} had different responses to climate factors across various climatic zones in China. Wang et al. [42] declared the decreasing net radiation was responsible for the ET_{ref} decrease in the three-river source area in China. The significantly increasing TA was the main reason for decreasing ET_{ref} in the entire Yellow River Basin [21]. Thus, effects of climate factors on ET_{ref} need to be further analyzed, especially in areas with varied climatic conditions, such as the HRB. Even though outcomes of this research indicated that the sensitivity and quantitative contribution analysis can delineate the importance of model parameters to output findings, which allows using it for making an accurate prediction, the methods of sensitivity and quantitative contribution analysis can be extended to other regions.

4.3. Uncertainties

We have taken into consideration four main climate factors from the FAO-56 PM model and analyze their effects on ET_{ref} trends. Although we have developed the differential equation method by

using RH instead of e_a in this study to reduce the estimation error, some errors may still exist due these four meteorological parameters influencing each other to some extent. Meanwhile, the systematic and random errors, inherent in meteorological measurements, could also affect the values of climate factors for estimating ET_{ref} [87]. At the same time, the influence of anthropogenic activities has acted as a primary part in recent years (e.g., Peterson et al. [81], Wang et al. [37]) and more uncertain factors are rising. Furthermore, attention should be drawn to some of the uncertainties that exist in the partial derivatives of the ET_{ref} , such as relative and fluctuating values during the long-term study period. The mean values of the partial derivatives of each climatic factor were used to calculate the contributions to ET_{ref} in our study which might generate more uncertainties [43]. In addition, on account of the lack of observed solar radiation data, the empirical parameters (a_s, b_s) of the Angstrom equation listed in Equation (3) might have changed during the past 54 years' time series due to the changed aerosol optical thickness in this area [90]. This is a crucial indication and may also constrain the measured effects of the changes in SR on ET_{ref} , ultimately leading to the underestimation of results by adopting this approximate value for calculating solar radiation from sunshine duration [16].

5. Conclusions

We found the variation of ET_{ref} could not generate obvious spatial diversity, with the higher values concentrated in the north of middle HRB and Yi-Shu-Si River Basin. ET_{ref} showed a significant downward trend ($p < 0.001$) in the upper and middle HRB, and also the Yi-Shu-Si River Basin, particularly in summer and during the growing season, while ET_{ref} exhibited a slight increasing trend in the lower HRB, especially significantly in spring. All these phenomena could be explained reasonably by the variations in climate factors. TA had a significant upward trend in most time scales except in summer; RH fluctuated obviously and showed a significant decreasing trend in the lower HRB in each time scale; WS exhibited a significant decreasing trend in all sub-regions in each time scale; and SR had a significant downward trend in most time scales, except in spring. According to the sensitivities of ET_{ref} to climate factors in the HRB, the negative RH showed as the most sensitive factor in most sub-regions, with the positive $SR, TA,$ and WS following, respectively. However, the ET_{ref} was most sensitive to SR in the growing season and summer in most sub-regions except the lower HRB. Based on the developed differential equation method, WS was the most contributing factor, followed by $SR, TA,$ and RH in most time scales, while the SR contributed most to the ET_{ref} trends in growing season and summer in most sub-regions, except the lower HRB. Generally, the negative contribution values of the WS and SR would offset the positive ones of TA and RH , which lead to an overall significant decreasing trend in ET_{ref} in relevant sub-regions and time scales. However, in the lower HRB, the RH contributed most to ET_{ref} , with $WS, TA,$ and SR following, which could be responsible for the slightly increasing trend in ET_{ref} here.

This research deepens insights into the change patterns of regional climate and ET_{ref} , which will offer a scientific theoretical foundation for future investigation on the actual evapotranspiration (ET) of this basin. This research also plays a pivotal role in analogical agricultural crop production and irrigation management. The estimation of ET by using the physical model, as well as remote sensing and land use data, in recent years is an important study, which will delineate the spatiotemporal patterns of ET and its controlling factors in the HRB in the context of rapid urbanization and climatic change. It deserves further investigation and can be a promising extension of this present research work.

Acknowledgments: The fund of this research comes from the Postgraduate Research & Practice Innovation Program of Jiangsu Province (KYCX17_0885) and China Special Fund for Meteorological Research in the Public Interest (GYHY201106043; GYHY201506001). We also thank the editors and two anonymous reviewers for their constructive comments and suggestions that helped us to improve the quality of this manuscript.

Author Contributions: Meng Li and Ronghao Chu analyzed the data and wrote the paper. Shuanghe Shen supervised the whole research. Abu Reza Md. Towfiqul Islam modified and polished the English in this paper.

Conflicts of Interest: The authors declare no conflict of interest.

Appendix A. Validation of the Hargreaves–Samani Method for Estimating Solar Radiation

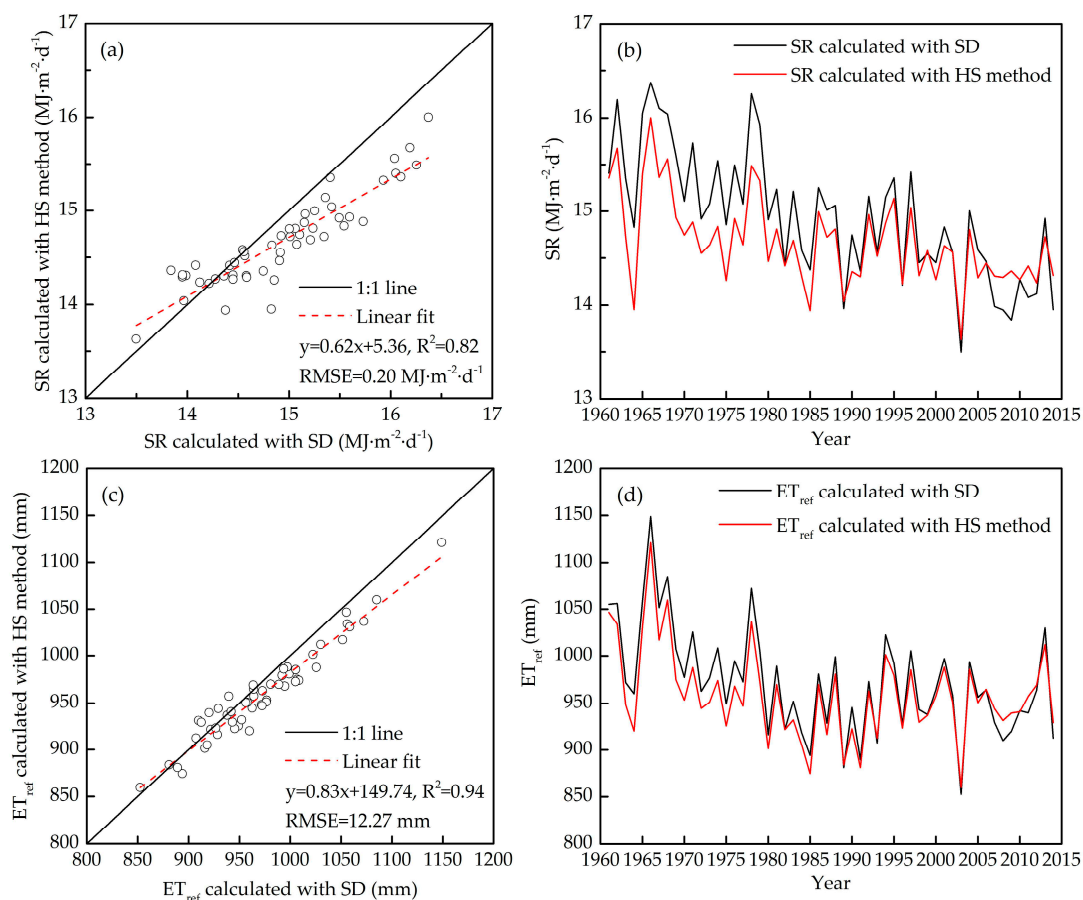


Figure A1. (a) The fitting precision of the SR_{HS} (SR calculated with Hargreaves–Samani method), (b) compared with the SR_{SD} (SR calculated with SD), and (c) the fitting precision of ET_{ref_HS} (ET_{ref} calculated with Hargreaves–Samani method) compared with (d) the ET_{ref_SD} (ET_{ref} calculated with SD).

References

- Xu, C.Y.; Gong, L.; Jiang, T.; Chen, D.; Singh, V.P. Analysis of spatial distribution and temporal trend of reference evapotranspiration and pan evaporation in Changjiang (Yangtze River) catchment. *J. Hydrol.* **2006**, *327*, 81–93. [[CrossRef](#)]
- Allen, R.G.; Pereira, L.S.; Raes, D.; Smith, M. *Crop Evapotranspiration—Guidelines for Computing Crop Water Requirements—FAO Irrigation and Drainage Paper 56*; FAO: Rome, Italy, 1998.
- Zhao, L.; Xia, J.; Sobkowiak, L.; Li, Z. Climatic Characteristics of Reference Evapotranspiration in the Hai River Basin and Their Attribution. *Water* **2014**, *6*, 1482–1499. [[CrossRef](#)]
- Thomas, A. Development and properties of 0.25-degree gridded evapotranspiration data fields of China for hydrological studies. *J. Hydrol.* **2008**, *358*, 145–158. [[CrossRef](#)]
- Jhajharia, D.; Shrivastava, S.K.; Sarkar, D.; Sarkar, S. Temporal characteristics of pan evaporation trends under the humid conditions of northeast India. *Agric. For. Meteorol.* **2009**, *149*, 763–770. [[CrossRef](#)]
- Zuo, H.; Chen, B.; Wang, S.; Guo, Y.; Zuo, B.; Wu, L.; Gao, X. Observational study on complementary relationship between pan evaporation and actual evapotranspiration and its variation with pan type. *Agric. For. Meteorol.* **2016**, *222*, 1–9. [[CrossRef](#)]
- Alexander, L.V.; Allen, S.K.; Bindoff, N.L.; Bréon, F.-M.; Church, J.A.; Cubasch, U.; Emori, S.; Forster, P.; Friedlingstein, P.; Gillett, N.; et al. Climate change 2013: The physical science basis, in contribution of Working Group I (WGI) to the Fifth Assessment Report (AR5) of the Intergovernmental Panel on Climate Change (IPCC). *Science* **2013**, *129*, 83–103.

8. Xu, L.; Shi, Z.; Wang, Y.; Zhang, S.; Chu, X.; Yu, P.; Xiong, W.; Zuo, H.; Wang, Y. Spatiotemporal variation and driving forces of reference evapotranspiration in Jing River Basin, northwest China. *Hydrol. Process.* **2015**, *29*, 4846–4862. [[CrossRef](#)]
9. McMahon, T.A.; Finlayson, B.L.; Peel, M.C. Historical developments of models for estimating evaporation using standard meteorological data. *WIREs Water* **2016**, *3*, 788–818. [[CrossRef](#)]
10. Cong, Z.T.; Yang, D.W.; Ni, G.H. Does evaporation paradox exist in China? *Hydrol. Earth Syst. Sci.* **2009**, *13*, 357–366. [[CrossRef](#)]
11. Limjirakan, S.; Limsakul, A. Trends in Thailand pan evaporation from 1970 to 2007. *Atmos. Res.* **2012**, *108*, 122–127. [[CrossRef](#)]
12. Breña-Naranjo, J.A.; Laverde-Barajas, M.Á.; Pedrozo-Acuña, A. Changes in pan evaporation in Mexico from 1961 to 2010. *Int. J. Climatol.* **2016**, *23*, 361–387. [[CrossRef](#)]
13. Brutsaert, W.; Parlange, M.B. Hydrologic cycle explains the evaporation paradox. *Nature* **1998**, *396*, 30. [[CrossRef](#)]
14. Huo, Z.; Dai, X.; Feng, S.; Kang, S.; Huang, G. Effect of climate change on reference evapotranspiration and aridity index in arid region of China. *J. Hydrol.* **2013**, *492*, 24–34. [[CrossRef](#)]
15. Thomas, A. Spatial and temporal characteristics of potential evapotranspiration trends over China. *Int. J. Climatol.* **2000**, *20*, 381–396. [[CrossRef](#)]
16. Chu, R.; Li, M.; Shen, S.; Islam, A.R.M.T.; Cao, W.; Tao, S.; Gao, P. Changes in reference evapotranspiration and its contributing factors in Jiangsu, a major economic and agricultural province of eastern China. *Water* **2017**, *9*, 486. [[CrossRef](#)]
17. Dinpashoh, Y.; Jhajharia, D.; Fard, A.F.; Singh, V.P.; Kahya, E. Trends in reference crop evapotranspiration over Iran. *J. Hydrol.* **2011**, *399*, 422–433. [[CrossRef](#)]
18. Tabari, H.; Aghajanjoo, M.B. Temporal pattern of aridity index in Iran with considering precipitation and evapotranspiration trends. *Int. J. Climatol.* **2013**, *33*, 396–409. [[CrossRef](#)]
19. Chauouche, K.; Neppel, L.; Dieulin, C.; Pujol, N.; Ladouche, B.; Martin, E.; Salas, D.; Caballero, Y. Analyses of precipitation, temperature and evapotranspiration in a French Mediterranean region in the context of climate change. *Comptes Rendus Geosci.* **2010**, *342*, 234–243. [[CrossRef](#)]
20. Palumbo, A.D.; Vitale, D.; Campi, P.; Mastroianni, M. Time trend in reference evapotranspiration: Analysis of a long series of agrometeorological measurements in Southern Italy. *Irrig. Drain. Syst.* **2011**, *25*, 395–411. [[CrossRef](#)]
21. Liu, Q.; Yang, Z.; Cui, B.; Sun, T. The temporal trends of reference evapotranspiration and its sensitivity to key meteorological variables in the Yellow River Basin, China. *Hydrol. Process.* **2010**, *24*, 2171–2181. [[CrossRef](#)]
22. Zuo, D.; Xu, Z.; Yang, H.; Liu, X. Spatiotemporal variations and abrupt changes of potential evapotranspiration and its sensitivity to key meteorological variables in the Wei River basin, China. *Hydrol. Process.* **2012**, *26*, 1149–1160. [[CrossRef](#)]
23. Vörösmarty, C.J.; Sahagian, D. Anthropogenic disturbance of the terrestrial water cycle. *Bioscience* **2000**, *50*, 753–765. [[CrossRef](#)]
24. Rezaei, M.; Valipour, M.; Valipour, M. Modelling evapotranspiration to increase the accuracy of the estimations based on the climatic parameters. *Water Conserv. Sci. Eng.* **2016**, *1*, 197–207. [[CrossRef](#)]
25. Valipour, M.; Sefidkouhi, M.A.G.; Sarjaz, M.R. Selecting the best model to estimate potential evapotranspiration with respect to climate change and magnitudes of extreme events. *Agric. Water Manag.* **2017**, *180*, 50–60. [[CrossRef](#)]
26. Tegos, A.; Malamos, N.; Efstratiadis, A.; Tsoukalas, I.; Karanasios, A.; Koutsoyiannis, D. Parametric Modelling of Potential Evapotranspiration: A Global Survey. *Water* **2017**, *9*, 795. [[CrossRef](#)]
27. McCuen, R.H. A sensitivity and error analysis of procedures used for estimating evaporation. *J. Am. Water Resour. Assoc.* **1974**, *10*, 486–497. [[CrossRef](#)]
28. Yin, Y.; Wu, S.; Chen, G.; Dai, E. Attribution analyses of potential evapotranspiration changes in China since the 1960s. *Theor. Appl. Climatol.* **2010**, *101*, 19–28. [[CrossRef](#)]
29. Fan, J.; Wu, L.; Zhang, F.; Xiang, Y.; Zheng, J. Climate change effects on reference crop evapotranspiration across different climatic zones of China during 1956–2015. *J. Hydrol.* **2016**, *542*, 923–937. [[CrossRef](#)]
30. Gao, Z.; He, J.; Dong, K.; Bian, X.; Li, X. Sensitivity study of reference crop evapotranspiration during growing season in the West Liao River basin, China. *Theor. Appl. Climatol.* **2016**, *124*, 1–17. [[CrossRef](#)]

31. Li, C.; Wu, P.T.; Li, X.L.; Zhou, T.W.; Sun, S.K.; Wang, Y.B.; Luan, X.B.; Yu, X. Spatial and temporal evolution of climatic factors and its impacts on potential evapotranspiration in Loess Plateau of Northern Shaanxi, China. *Sci. Total Environ.* **2017**, *589*, 165–172. [[CrossRef](#)] [[PubMed](#)]
32. Ye, X.; Li, X.; Liu, J.; Xu, C.; Zhang, Q. Variation of reference evapotranspiration and its contributing climatic factors in the Poyang Lake catchment, China. *Hydrol. Process.* **2015**, *28*, 6151–6162. [[CrossRef](#)]
33. Shan, N.; Shi, Z.; Yang, X.; Gao, J.; Cai, D. Spatiotemporal trends of reference evapotranspiration and its driving factors in the Beijing-Tianjin Sand Source Control Project Region, China. *Agric. For. Meteorol.* **2015**, *200*, 322–333. [[CrossRef](#)]
34. Wang, Z.; Xie, P.; Lai, C.; Chen, X.; Wu, X.; Zeng, Z.; Li, J. Spatiotemporal variability of reference evapotranspiration and contributing climatic factors in China during 1961–2013. *J. Hydrol.* **2017**, *544*, 97–108. [[CrossRef](#)]
35. Gao, Z.; He, J.; Dong, K.; Li, X. Trends in reference evapotranspiration and their causative factors in the West Liao River basin, China. *Agric. For. Meteorol.* **2017**, *232*, 106–177. [[CrossRef](#)]
36. Li, Z.; Li, Z.; Xu, Z.; Zhou, X. Temporal variations of reference evapotranspiration in Heihe River basin of China. *Hydrol. Res.* **2013**, *44*, 904–916. [[CrossRef](#)]
37. Wang, W.; Shao, Q.; Peng, S.; Xing, W.; Yang, T.; Luo, Y.; Yong, B.; Xu, J. Reference evapotranspiration change and the causes across the Yellow River Basin during 1957–2008 and their spatial and seasonal differences. *Water Resour. Res.* **2012**, *48*, 1–27. [[CrossRef](#)]
38. Nouri, M.; Homaei, M.; Bannayan, M. Quantitative trend, sensitivity and contribution analyses of reference evapotranspiration in some arid environments under climate change. *Water Resour. Manag.* **2017**, *31*, 2207–2224. [[CrossRef](#)]
39. Roderick, M.L.; Rotstayn, L.D.; Farquhar, G.D.; Hobbins, M.T. On the attribution of changing pan evaporation. *Geophys. Res. Lett.* **2007**, *34*, 251–270. [[CrossRef](#)]
40. Zheng, H.; Liu, X.; Liu, C.; Dai, X.; Zhu, R. Assessing contributions to pan evaporation trends in Haihe River Basin, China. *J. Geophys. Res.* **2009**, *114*, 144–153. [[CrossRef](#)]
41. Liu, Q.; Mcvicar, T.R. Assessing climate change induced modification of Penman potential evaporation and runoff sensitivity in a large water-limited basin. *J. Hydrol.* **2012**, *464–465*, 352–362. [[CrossRef](#)]
42. Wang, Q.; Wang, J.; Zhao, Y.; Li, H.; Zhai, J.; Yu, Z.; Zhang, S. Reference evapotranspiration trends from 1980 to 2012 and their attribution to meteorological drivers in the three-river source region, China. *Int. J. Climatol.* **2016**, *36*, 3759–3769. [[CrossRef](#)]
43. Liu, X.; Zhang, D. Trend analysis of reference evapotranspiration in Northwest China: The roles of changing wind speed and surface air temperature. *Hydrol. Process.* **2013**, *27*, 3941–3948. [[CrossRef](#)]
44. Ye, J.; He, Y.; Pappenberger, F.; Cloke, H.L.; Manful, D.; Li, Z. Evaluation of ECMWF medium-range ensemble forecasts of precipitation for river basins. *Q. J. R. Meteorol. Soc.* **2013**, *140*, 1615–1628. [[CrossRef](#)]
45. Yan, J.; Yu, J.; Tao, G.; Vos, J.; Bouman, B.A.M.; Xie, G.H.; Meinke, H. Yield formation and tillering dynamics of direct-seeded rice in flooded and nonflooded soils in the Huai River Basin of China. *Field Crop. Res.* **2010**, *116*, 252–259. [[CrossRef](#)]
46. Angstrom, A. Solar and terrestrial radiation. Report to the international commission for solar research on actinometric investigations of solar and atmospheric radiation. *Q. J. R. Meteorol. Soc.* **1924**, *50*, 121–126. [[CrossRef](#)]
47. Chen, R.; Kang, E.; Yang, J.; Lu, S.; Zhao, W. Validation of five global radiation models with measured daily data in China. *Energy Convers. Manag.* **2004**, *45*, 1759–1769. [[CrossRef](#)]
48. Hargreaves, G.H.; Samani, Z.A. Estimating potential evapotranspiration. *J. Irrig. Drain. Div.* **1982**, *108*, 225–230.
49. Hargreaves, G.H.; Allen, R.G. History and evaluation of Hargreaves evapotranspiration equation. *J. Irrig. Drain. Eng.* **2003**, *129*, 53–63. [[CrossRef](#)]
50. Allen, R.G. Self-Calibrating Method for Estimating Solar Radiation from Air Temperature. *J. Hydrol. Eng.* **1997**, *2*, 56–67. [[CrossRef](#)]
51. Tabari, H.; Somee, B.S.; Zadeh, M.R. Testing for long-term trends in climatic variables in Iran. *Atmos. Res.* **2011**, *100*, 132–140. [[CrossRef](#)]
52. Zhang, Q.; Liu, C.; Xu, C.; Xu, Y.; Jiang, T. Observed trends of annual maximum water level and streamflow during past 130 years in the Yangtze River basin, China. *J. Hydrol.* **2006**, *324*, 255–265. [[CrossRef](#)]
53. Mann, H.B. Nonparametric test against trend. *Econometrica* **1945**, *13*, 245–259. [[CrossRef](#)]
54. Kendall, M.G. *Rank Correlation Methods*; Griffin: London, UK, 1975.
55. Theil, H. *A Rank Invariant Method of Linear and Polynomial Regression Analysis*; Nederlandse Akademie Van Wetenschappen: Amsterdam, The Netherlands, 1950.

56. Sen, P.K. Estimates of the Regression Coefficient Based on Kendall's Tau. *J. Am. Stat. Assoc.* **1968**, *63*, 1379–1389. [[CrossRef](#)]
57. Von Storch, H.; Navarra, A. *Analysis of Climate Variability: Applications of Statistical Techniques, Misuses of Statistical Analysis in Climate Research*; Springer: Berlin, Germany, 1995.
58. Yue, S.; Pilon, P.; Phinney, B.; Cavadias, G. The influence of autocorrelation on the ability to detect trend in hydrological series. *Hydrol. Process.* **2002**, *16*, 1807–1829. [[CrossRef](#)]
59. Kumar, S.; Merwade, V.; Kam, J.; Thurner, K. Streamflow trends in Indiana: Effects of long term persistence, precipitation and subsurface drains. *J. Hydrol.* **2009**, *374*, 171–183. [[CrossRef](#)]
60. Tegos, A.; Malamos, N.; Koutsoyiannis, D. A parsimonious regional parametric evapotranspiration model based on a simplification of the Penman-Monteith formula. *J. Hydrol.* **2015**, *524*, 708–717. [[CrossRef](#)]
61. Zhao, C.; Nan, Z.; Cheng, G. Methods for modelling of temporal and spatial distribution of air temperature at landscape scale in the southern Qilian mountains, China. *Ecol. Model.* **2005**, *189*, 209–220.
62. Sun, F.; Yang, X.; Lu, S.; Yang, S. The contrast analysis on the average and extremum temperature trend in Northeast China. *Sci. Meteorol. Sin.* **2006**, *26*, 157–163.
63. McVicar, T.R.; Roderick, M.L.; Donohue, R.J.; Li, L.T.; Niel, T.G.V.; Thomas, A.; Grieser, J.; Jhajharia, D.; Himri, Y.; Mahowald, N.M.; et al. Global review and synthesis of trends in observed terrestrial near-surface wind speeds: Implications for evaporation. *J. Hydrol.* **2012**, *416–417*, 182–205. [[CrossRef](#)]
64. Guo, H.; Xu, M.; Hu, Q. Changes in near-surface wind speed in China: 1969–2005. *Int. J. Climatol.* **2015**, *31*, 349–358. [[CrossRef](#)]
65. McVicar, T.R.; Roderick, M.L. Atmospheric science: Winds of change. *Nat. Geosci.* **2010**, *3*, 747–748. [[CrossRef](#)]
66. Song, Z.W.; Zhang, H.L.; Snyder, R.L.; Anderson, F.E.; Chen, F. Distribution and trends in reference evapotranspiration in the North China Plain. *J. Irrig. Drain. Eng.* **2010**, *136*, 240–247. [[CrossRef](#)]
67. Vautard, R.; Cattiaux, J.; Yiou, P.; Thépaut, J.-N.; Ciais, P. Northern Hemisphere atmospheric stilling partly attributed to an increase in surface roughness. *Nat. Geosci.* **2010**, *3*, 756–761. [[CrossRef](#)]
68. Shi, Z.; Xu, L.; Yang, X.; Guo, H.; Dong, L.; Song, A.; Zhang, X.; Shan, N. Trends in reference evapotranspiration and its attribution over the past 50 years in the Loess Plateau, China: Implications for ecological projects and agricultural production. *Stoch. Environ. Res. Risk Assess.* **2017**, *31*, 257–273. [[CrossRef](#)]
69. Xu, M.; Chang, C.-P.; Fu, C.; Qi, Y.; Robock, A.; Robinson, D.; Zhang, H.-M. Steady decline of East Asian monsoon winds, 1969–2000: Evidence from direct ground measurements of wind speed. *J. Geophys. Res.* **2006**, *111*, 906–910. [[CrossRef](#)]
70. You, Q.; Kang, S.; Flügel, W.-A.; Pepin, N.; Yan, Y.; Huang, J. Decreasing wind speed and weakening latitudinal surface pressure gradients in the Tibetan Plateau. *Clim. Res.* **2010**, *42*, 57–64. [[CrossRef](#)]
71. Lin, C.; Yang, K.; Qin, J. Observed surface and upper-air wind speed changes over China since 1960. *J. Clim.* **2012**, *26*, 2891–2903. [[CrossRef](#)]
72. Kwon, M.H.; Jhun, J.G.; Ha, K.J. Decadal change in East Asian summer monsoon circulation in the mid-1990s. *Geophys. Res. Lett.* **2007**, *34*, 377–390. [[CrossRef](#)]
73. Teh, C.B.S. *Introduction to Mathematical Modeling of Crop Growth: How the Equations Are Derived and Assembled into a Computer Program*; BrownWalker Press: Boca Raton, FL, USA, 2006.
74. Stanhill, G.; Cohen, S. Global dimming: A review of the evidence for a widespread and significant reduction in global radiation with discussion of its probable causes and possible agricultural consequences. *Agric. For. Meteorol.* **2001**, *107*, 255–278. [[CrossRef](#)]
75. Liepert, B.G. Observed reductions of surface solar radiation at sites in the United States and worldwide from 1961 to 1990. *Geophys. Res. Lett.* **2002**, *29*, 1–4. [[CrossRef](#)]
76. Wild, M.; Gilgen, H.; Roesch, A.; Ohmura, A.; Long, C.N.; Dutton, E.G.; Forgan, B.; Kallis, A.; Russak, V.; Tsvetkov, A. From dimming to brightening: Decadal changes in solar radiation at Earth's surface. *Science* **2005**, *308*, 847–850. [[CrossRef](#)] [[PubMed](#)]
77. Stjern, C.W.; Ansson, J.E.K.; Hansen, A.W. Global dimming and global brightening-an analysis of surface radiation and cloud cover data in northern Europe. *Int. J. Climatol.* **2008**, *29*, 643–653. [[CrossRef](#)]
78. Qian, Y.; Wang, W.; Leung, L.R.; Kaiser, D.P. Variability of solar radiation under cloud-free skies in China: The role of aerosols. *Geophys. Res. Lett.* **2007**, *34*, 1–5. [[CrossRef](#)]
79. Che, H.Z.; Shi, G.Y.; Zhang, X.Y.; Arimoto, R.; Zhao, J.Q.; Xu, L.; Wang, B.; Chen, Z.H. Analysis of 40 years of solar radiation data from China, 1961–2000. *Geophys. Res. Lett.* **2005**, *32*, 1–5. [[CrossRef](#)]

80. Yang, Y.H.; Zhao, N.; Hu, Y.K.; Zhou, X.Y. Effect of wind speed on sunshine hours in three cities in northern China. *Clim. Res.* **2009**, *39*, 149–157. [[CrossRef](#)]
81. Peterson, T.C.; Golubev, V.S.; Groisman, P.Y. Evaporation losing its strength. *Nature* **1995**, *377*, 687–688. [[CrossRef](#)]
82. Goyal, R.K. Sensitivity of evapotranspiration to global warming: A case study of arid zone of Rajasthan (India). *Agric. Water Manag.* **2004**, *69*, 1–11. [[CrossRef](#)]
83. Hulme, M.; Zhao, Z.; Jiang, T. Recent and future climate change in East Asia. *Int. J. Climatol.* **1994**, *14*, 637–658. [[CrossRef](#)]
84. Tang, B.; Tong, L.; Kang, S.; Zhang, L. Impacts of climate variability on reference evapotranspiration over 58 years in the Haihe river basin of north China. *Agric. Water Manag.* **2011**, *97*, 1506–1516. [[CrossRef](#)]
85. Roderick, M.L.; Farquhar, G.D. Changes in Australian pan evaporation from 1970 to 2002. *Int. J. Climatol.* **2004**, *24*, 1077–1090. [[CrossRef](#)]
86. Gong, L.; Xu, C.-Y.; Chen, D.; Halldin, S.; Chen, Y.D. Sensitivity of the Penman-Monteith reference evapotranspiration to key climatic variables in the Changjiang (Yangtze River) basin. *J. Hydrol.* **2006**, *329*, 620–629. [[CrossRef](#)]
87. Estévez, J.; Gavilán, P.; Berengena, J. Sensitivity analysis of a Penman–Monteith type equation to estimate reference evapotranspiration in Southern Spain. *Hydrol. Process.* **2009**, *23*, 3342–3353. [[CrossRef](#)]
88. Irmak, S.; Payero, J.; Martin, D.; Irmak, A.; Howell, T. Sensitivity analyses and sensitivity coefficients of standardized daily ASCE-Penman-Monteith equation. *J. Irrig. Drain. Eng.* **2006**, *132*, 564–578. [[CrossRef](#)]
89. Zhang, Y.; Liu, C.; Tan, Y.; Yang, Y. Trends in pan evaporation and reference and actual evapotranspiration across the Tibetan Plateau. *J. Geophys. Res.* **2007**, *112*, 1–12. [[CrossRef](#)]
90. Li, M.; Chu, R.; Shen, S.; Islam, A.R.M.T. Dynamic analysis of pan evaporation variations in the Huai River Basin, a climate transition zone in eastern China. *Sci. Total Environ.* **2018**, *625*, 496–509. [[CrossRef](#)] [[PubMed](#)]



© 2018 by the authors. Licensee MDPI, Basel, Switzerland. This article is an open access article distributed under the terms and conditions of the Creative Commons Attribution (CC BY) license (<http://creativecommons.org/licenses/by/4.0/>).